Impact of unidentified light charged hadron data on the determination of pion fragmentation functions

Maryam Soleymaninia,[1,3,*] Muhammad Goharipour,[3,†] and Hamzeh Khanpour[2,3,‡]

[1]*Institute of Advanced Technologies, Shahid Rajaee Teacher Training University, Lavizan, Tehran, 16788, Iran*
[2]*Department of Physics, University of Science and Technology of Mazandaran, P.O. Box 48518-78195, Behshahr, Iran*
[3]*School of Particles and Accelerators, Institute for Research in Fundamental Sciences (IPM), P.O. Box 19395-5531, Tehran, Iran*

In this paper a new comprehensive analysis of parton-to-pion fragmentation functions (FFs) is performed for the first time by including all experimental datasets on single inclusive pion as well as unidentified light charged hadron production in electron-positron ($e^+ e^-$) annihilation. We determine the pion FFs along with their uncertainties using the standard "Hessian" technique at next-to-leading order (NLO) and next-to-next-to-leading order (NNLO) in perturbative QCD. It is shown that the determination of pion FFs using simultaneously the datasets from pion and unidentified light charged hadron production leads to the reduction of all pion FF uncertainties, especially for the case of strange quark and gluon FFs by significant factors. In this study, we have quantified the constraints that these datasets could impose on the extracted pion FFs. Our results also illustrate the significant improvement in the precision of FFs fits achievable by the inclusion of higher-order corrections. The improvements on FF uncertainties as well as fit quality have been clearly discussed.

I. INTRODUCTION

Essential ingredients of theoretical predictions for present or future hadron colliders, such as the large hadron collider (LHC) and large hadron-electron collider (LHeC), are the detailed understanding of the quark and gluon structure of the nucleon [1–4]. These are quantified by the parton distribution functions (PDFs) [5–7] as well as the fragmentation functions (FFs) [8–20]. In recent years, the precise determination of PDFs as well as FFs, including their experimental uncertainties, had become an active topic for many LHC processes, including the top quark and Higgs boson sectors, searches for new heavy beyond-the-Standard-Model (BSM) particles, and searches for new physics (NP), as well as in the measurement of fundamental SM parameters such as the strong coupling constant. For more details, we refer the readers to the literature [21–23] and a recent study on the PDFs at the high-luminosity LHC (HL-LHC) [1].

In a hard-scattering collision, PDFs determine how the proton's momentum is shared among its constituents. Likewise, the FFs describe the probability density for the fragmentation of the final-state parton with a certain momentum into the hadron with a fraction of the parton's momentum. PDFs and the FFs depend on the factorization scale. This dependence is described by the Dokshitzer-Gribov-Lipatov-Altarelli-Parisi (DGLAP) evolution equations [24–27], which allow the calculation of the PDFs and FFs if they are known at a given initial scale, i.e., $\mu^2 = \mu_0^2$. It is well known that the PDFs and the FFs cannot be calculable in perturbation theory, and hence, these distributions need to be extracted from experimental information through a QCD fit. In addition, these nonperturbative functions are also universal. The universality of PDFs and FFs commonly refers to the fact that, since the hadronization processes are not sensitive to the particular choices of a hard-scattering process at short range, these nonperturbative functions can be extracted from a certain kind of scattering experimental observables. Then the extracted distributions can be used for the theory predictions of scattering observable in high-energy collisions.

New and precise datasets are vital for the precise determination of FFs. These datasets have been and are currently being collected from different high-energy processes at a variety of lepton and hadron colliders. These processes

include the hadron production data in single-inclusive electron-positron (e^+e^-) annihilation (SIA), semi-inclusive deep inelastic scattering (SIDIS), and proton-proton and proton-antiproton collisions measured by TEVATRON, RHIC, and LHC. For a list of all available datasets, we refer the readers to the recent analysis by the NNPDF Collaboration and references therein [8,9]. Several analyses have been done so far to extract FFs using the observables mentioned above. Among them are the recent determination of charged hadron FFs from collider data by the NNPDF Collaboration (NNFF1.1h) [8]. This collaboration has also determined the pions, kaons, and proton FFs using the SIA datasets at NNLO in perturbative QCD based on the NNPDF methodology (NNFF1.0) [9]. The recent analyses by HKKS16 [13] and JAM16 [28] also have been performed using the SIA data only. Other analyses in literature can be found, for example, in Refs. [29–36]

Recently, we also have performed the first determination of $D^{*\pm}$-meson FFs and their uncertainties at NNLO (SKM18) [10]. In Ref. [11], we presented our QCD analysis of charged hadron FFs and their uncertainties at NLO and NNLO (SGK18), which is the first determination of light charged hadron FFs at NNLO accuracy. Finally, in Ref. [12], the contributions from *residual* light charged hadrons in the inclusive charged hadrons have been extracted using the e^+e^- annihilation datasets. Since the QCD framework for FFs at NNLO is not accessible for SIDIS and hadron-hadron collisions, both of our analyses are restricted to the single-inclusive charged hadron production in electron-positron annihilation. The uncertainties in our recent analyses on FFs, as well as the corresponding observables, are estimated using the "Hessian" technique.

In this work, an extraction of pion FFs from a QCD analysis of electron-positron annihilation experimental data in the zero-mass variable flavor number scheme (ZM-VFNS) has been presented. The main aim of this paper is to examine, for the first time, the impact of unidentified light charged hadron experimental data on the determination of pion FFs and their uncertainties at NLO and NNLO accuracy. In this respect, we have attempted a determination of pion FFs considering two different scenarios. First, we present a determination of pion FFs through a QCD analysis of pion datasets. In this first study of FFs, which is performed within ZM-VFNS at both NLO and NNLO approximations and referred to as the "pion fit," we simplify the analysis by considering the pion datasets only. Second, we determine pion FFs through a QCD analysis by including both pion and unidentified light charged hadron datasets. We show that simultaneously fitting the pion FFs using both datasets leads to a well-constrained determination of pion FFs, including significant effect on the extracted uncertainties. Our second fit is called the "pion + hadron fit."

The outline of this paper is as follows: In Sec. II, we present in detail all available SIA datasets for pion production, as well as the SIA datasets for the unidentified light charged hadrons. In Sec. III, we discuss the theoretical formalism of single-hadron inclusive production in electron-positron (e^+e^-) annihilation. This section also includes detailed discussions of our fitting process and parametrization for the pion FFs. Section IV is then dedicated to our results. The obtained results are clearly discussed for variety of aspect in this section, and comparisons with other analyses in literature are also presented. This section also includes our theory predictions based on the extracted pion FFs, including a comparison with all data analyzed. Finally, Sec. V includes a summary and our conclusions.

II. EXPERIMENTAL DATA SELECTION

In this section, we present the experimental datasets that are included in our "pion fit" and "pion + hadron fit" analyses. As we mentioned in the Introduction, our QCD fits are performed by inducing the electron-positron annihilation data in two scenarios: In the first analysis, we use the available SIA data for pions from Refs. [37–46] to extract the pion FFs. In the second analysis, the SIA datasets for the unidentified charged hadrons [41,44, 46–51] along with the pion datasets, are included in our fits to calculate the pion FFs. All the datasets for pion and unidentified hadrons are listed in Tables I and II for inclusive and flavor-tagged SIA data, which are reported by different experiments. Note that the measured observables for these datasets, especially for the pion, are different—a complete explanation about SIA pion data and the relations between the scaling variables is available in related analysis performed by the NNPDF Collaboration in NNFF1.0 [9]. In addition, we have used the unidentified light charged hadron experimental data in our recent study of SGK18 [11]. The details of corrections to these datasets and the kinematic cuts applied are presented in Ref. [11].

According to the datasets presented in the second column of Tables I and II, the observables are different and provide limited sensitivity to the separation between light and heavy quark FFs due to the flavor-tagged data. Since the gluon receives its leading-order (LO) accuracy at $\mathcal{O}(\alpha_s)$, the total SIA cross sections are poor for constraining this density. However, the longitudinal cross sections can impose a comparable sensitivity to the gluon FF, because the longitudinal coefficient functions start at $\mathcal{O}(\alpha_s)$. Hence, the longitudinal observables that are available for the unidentified hadrons could constrain the gluon FF well enough. It should be noted that the NNLO QCD corrections for longitudinal structure functions are not available in the literature, and hence, such corrections cannot be considered in our analyses.

In this paper, we plan to study the effects arising from the unidentified light charged hadron experimental data on the calculation of pion FFs by including both pion and unidentified hadron datasets, and then comparing the

TABLE I.　The datasets included in the analyses of $\pi^{\pm}$ FFs at NLO. For each experiment, we indicate the corresponding reference, the measured observables, the center-of-mass energy $\sqrt{s}$, and the χ^2/pts values for every dataset, as well as the total χ^2/d.o.f.

Dataset	Observable	$\sqrt{s}$ [GeV]	χ^2/pts "pion"	χ^2/pts "pion + hadron"
BELLE [37]	inclusive	10.52	38.37/70	42.28/70
BABAR [38]	inclusive	10.54	78.07/40	81.64/40
TASSO12 [39]	inclusive	12	4.24/4	4.05/4
TASSO14 [40]	inclusive	14	11.76/9	12.04/9
TASSO22 [40]	inclusive	22	25.39/8	26.55/8
TPC [41]	inclusive	29	7.05/13	8.25/13
TASSO34 [42]	inclusive	34	19.22/9	23.26/9
TASSO44 [42]	inclusive	44	18.21/6	19.95/6
ALEPH [43]	inclusive	91.2	37.77/23	43.07/23
DELPHI [44]	inclusive	91.2	27.52/21	22.86/21
	uds tag	91.2	21.47/21	22.70/21
	b tag	91.2	21.12/21	11.11/21
OPAL [45]	inclusive	91.2	32.01/24	37.41/24
SLD [46]	inclusive	91.2	57.87/34	76.20/34
	uds tag	91.2	90.98/34	92.04/34
	c tag	91.2	38.83/34	40.13/34
	b tag	91.2	19.81/34	38.28/34
TASSO14 [47]	inclusive	14	$\cdots$	8.22/15
TASSO22 [47]	inclusive	22	$\cdots$	13.07/15
TPC [41]	inclusive	29	$\cdots$	20.72/21
TASSO35 [47]	inclusive	34	$\cdots$	21.74/15
TASSO44 [47]	inclusive	44	$\cdots$	18.80/15
ALEPH [48]	inclusive	91.2	$\cdots$	9.23/32
DELPHI [44,49]	inclusive	91.2	$\cdots$	16.86/22
	uds tag	91.2	$\cdots$	10.52/22
	b tag	91.2	$\cdots$	51.76/22
	Longitudinal inclusive	91.2	$\cdots$	28.49/20
	Longitudinal b tag	91.2	$\cdots$	20.12/20
OPAL [50,51]	inclusive	91.2	$\cdots$	12.40/20
	uds tag	91.2	$\cdots$	7.34/20
	c tag	91.2	$\cdots$	14.18/20
	b tag	91.2	$\cdots$	26.85/20
	Longitudinal inclusive	91.2	$\cdots$	89.18/20
SLD [46]	inclusive	91.2	$\cdots$	15.09/34
	uds tag	91.2	$\cdots$	15.86/34
	c tag	91.2	$\cdots$	29.26/34
	b tag	91.2	$\cdots$	81.21/34
Total χ^2/d.o.f.			1.42	1.44

extracted pion FFs with the results calculated from the QCD analysis using pion datasets alone. Since most of the contribution of FFs into the unidentified light charged hadron cross sections comes from the identified pion FFs, it motivates us to investigate the effect of unidentified light charged hadron datasets on the reduction of pion FF uncertainties. In Tables I and II, our results are reported at NLO and NNLO accuracies of perturbative QCD. In both tables, the fourth column presents our fit results for the value of χ^2 per number of data points (χ^2/N_{pts}) considering pion datasets in the fit, while in the fifth column the same quantity is reported considering both the pion and light hadron experimental datasets in the analysis. One of the most important findings from these tables is the

significant reduction of χ^2/d.o.f. by going from NLO to the NNLO corrections. We will return to this issue in the next section.

In order to avoid the sensitivity of behaviors of FF parametrization in the low and high regions of z, we apply cuts on the momentum fraction z. We exactly follow the cuts applied in our recent study on light charged hadron FFs, SGK18 [11]. These selections are also imposed for the pion experimental data. For datasets at $\sqrt{s} = M_Z$, we include the data points with the scaling variable of $z \geq 0.02$, and for $\sqrt{s} < M_Z$, the data points with $z \geq 0.075$ are included in our QCD fits. The data points with $z > 0.9$ are excluded in all of our QCD analyses. Considering the kinematical cut applied, the number of

TABLE II.   Same as Table I, but at NNLO accuracy.

Dataset	Observable	$\sqrt{s}$ [GeV]	χ^2/pts "pion"	χ^2/pts "pion + hadron"
BELLE [37]	inclusive	10.52	27.39/70	29.96/70
BABAR [38]	inclusive	10.54	59.84/40	57.80/40
TASSO12 [39]	inclusive	12	4.28/4	4.21/4
TASSO14 [40]	inclusive	14	11.50/9	11.67/9
TASSO22 [40]	inclusive	22	23.17/8	24.09/8
TPC [41]	inclusive	29	10.07/13	9.26/13
TASSO34 [42]	inclusive	34	14.44/9	15.93/9
TASSO44 [42]	inclusive	44	16.93/6	17.78/6
ALEPH [43]	inclusive	91.2	27.63/23	35.50/23
DELPHI [44]	inclusive	91.2	29.79/21	24.78/21
	uds tag	91.2	22.22/21	23.57/21
	b tag	91.2	19.96/21	10.57/21
OPAL [45]	inclusive	91.2	30.53/24	35.74/24
SLD [46]	inclusive	91.2	37.60/34	47.80/34
	uds tag	91.2	68.97/34	66.70/34
	c tag	91.2	31.73/34	35.18/34
	b tag	91.2	19.36/34	40.38/34
TASSO14 [47]	inclusive	14	$\cdots$	8.78/15
TASSO22 [47]	inclusive	22	$\cdots$	13.22/15
TPC [41]	inclusive	29	$\cdots$	15.69/21
TASSO35 [47]	inclusive	34	$\cdots$	23.33/15
TASSO44 [47]	inclusive	44	$\cdots$	19.41/15
ALEPH [48]	inclusive	91.2	$\cdots$	10.62/32
DELPHI [44,49]	inclusive	91.2	$\cdots$	18.55/22
	uds tag	91.2	$\cdots$	11.66/22
	b tag	91.2	$\cdots$	50.99/22
	Longitudinal inclusive	91.2	$\cdots$	9.47/20
	Longitudinal *b* tag	91.2	$\cdots$	9.37/20
OPAL [50,51]	inclusive	91.2	$\cdots$	14.23/20
	uds tag	91.2	$\cdots$	8.53/20
	c tag	91.2	$\cdots$	14.56/20
	b tag	91.2	$\cdots$	26.41/20
	Longitudinal inclusive	91.2	$\cdots$	7.99/20
SLD [46]	inclusive	91.2	$\cdots$	10.31/34
	uds tag	91.2	$\cdots$	10.97/34
	c tag	91.2	$\cdots$	29.74/34
	b tag	91.2	$\cdots$	80.62/34
Total χ^2/d.o.f.			1.17	1.06

data points is listed separately in the denominators of the fourth and fifth columns in Tables I and II for NLO and NNLO accuracy, respectively.

III. THEORETICAL METHODOLOGY FOR CALCULATIONS AND FITTING

In this section, a brief review of the theoretical framework and our methodology is presented. According to the factorization theorem, the SIA differential cross section normalized to the total cross section $\frac{1}{\sigma_{\text{tot}}}\frac{d\sigma^{H^{\pm}}}{dz}$ at a given center-of-mass energy of $\sqrt{S} = Q$ is written by

$$\frac{1}{\sigma_{\text{tot}}}\frac{d\sigma^{H^{\pm}}}{dz} = \frac{1}{\sigma_{\text{tot}}}[F_T^{H^{\pm}}(z,Q) + F_L^{H^{\pm}}(z,Q)]. \quad (1)$$

This equation is used for identified charged hadrons such as $\pi^{\pm}$, $K^{\pm}$, and $p/\bar{p}$, and for unidentified hadrons $h^{\pm}$. In Eq. (1), $H^{\pm}$ is defined as the sum of different charges of hadrons $H = H^+ + H^-$, and $z = \frac{2E_H}{\sqrt{s}}$ is the scaling variable. The total cross section σ_{tot} depends on the perturbative order of QCD corrections, and detailed explanations can be found, for example, in Ref. [11]. According to Eq. (1), in the case of multiplicities, the differential cross section for SIA processes can be decomposed into the timelike structure functions F_T and F_L, which are the transverse (T) and longitudinal (L) perturbative parts, respectively. The timelike structure functions can be written as convolutions of a perturbative part, the coefficient functions $C_i(z, \alpha_s)$, and a nonperturbative part, the FFs $D^{H^{\pm}}(z, Q)$:

$$F^{H^\pm}(z, Q) = \sum_i C_i(z, \alpha_s) \otimes D^{H^\pm}(z, Q). \qquad (2)$$

The coefficient functions have been calculated in Refs. [52–54], and they are available up to NNLO accuracy for electron-positron annihilations. It should be mentioned here that, in this analysis, the renormalization scale μ_R and the factorization scale μ_F are considered to be equal to the center-of-mass energy of collision, $\mu_R = \mu_F = \sqrt{s}$.

Since the universal FFs are nonperturbative functions, in order to determine the FFs, one needs to parametrize the functions of partons $i = q, \bar{q}, g$ at a given initial scale. The z parameter represents the fraction of the parton momentum which is carried by the hadron. Theoretically, the renormalization equations govern the scale dependence of the FFs, and they can be evaluated to a given higher-energy scale using the DGLAP evolution equations. In our analysis, we use the publicly available APFEL package [55] in order to calculate of the SIA cross sections, as well as the evolution of FFs by DGLAP equations, up to NNLO accuracy. In addition, the ZM-VFNS is considered to account for the heavy quark contributions, and hence, the effects of heavy quark mass are not taken into account in our analysis.

Our main aim in this analysis is to study the effect of adding all the experimental data for the unidentified light charged hadrons to that for the pions from SIA processes in the procedure of the determination of pion FFs. Hence, we need the theoretical definition of unidentified charge hadron FFs in our calculations. Experimentally, the unidentified light charged hadrons contain all identified light hadrons such as pions, kaons, protons, and small *residual* light hadrons. Then unidentified charged hadron cross sections of SIA can be calculated by summing the individual cross sections of the identified light ones ($\pi^\pm$, $K^\pm$, and $p/\bar{p}$) and the *residual* contribution. The SIA coefficient functions for all final states are the same, and hence, the FFs of unidentified light charged hadrons ($D^{h^\pm}$) can be defined as the sum of the pion, kaon, and proton FFs ($D^{\pi^\pm}$, $D^{K^\pm}$, $D^{p/\bar{p}}$), including the *residual* light hadron FFs $D^{\text{res}^\pm}$:

$$D^{h^\pm} = D^{\pi^\pm} + D^{K^\pm} + D^{p/\bar{p}} + D^{\text{res}^\pm}. \qquad (3)$$

Since our aim in this analysis is a new determination of pion FFs, $D^{\pi^\pm}$, we use the kaon and proton FFs from the NNFF1.0 parton set [9] at both NLO and NNLO accuracies. Recently, we have calculated the *residual* light hadron FFs $D^{\text{res}^\pm}$ in Ref. [12] up to NNLO QCD correction. In Ref. [12], we have shown that the contribution of the *residual* light hadrons is small, and hence, one can ignore this small contribution in Eq. (3). The contribution from this small distribution is not significant for the cases of total or light charged cross sections; however, for the cases of c- and b-tagged cross sections it is sizable.

For the uncertainty from NNFF1.0, we follow the analysis by DSS07 in Ref. [36] and estimate an average uncertainty of 5% in all theoretical calculations of the inclusive charged hadron cross sections stemming from the large uncertainties of kaon and proton FFs from the NNFF1.0 set. In addition, our recent study shows that an additional uncertainty due to the contributions of *residual* charged hadrons FFs [12] also needs to be taken into account. Overall, we believe that 8% of the cross section value seems to be reasonable. These additional uncertainties are included in the χ^2 minimization procedure for determining the pion FFs. In order to add these uncertainties, we apply the simplest way to include a "theory" error—we add it in quadrature to the statistical and systematic experimental error in the χ^2 expression. This is the standard approach that one can use to add this additional uncertainty to the QCD analysis. The methods of the present study are also consistent with those of DSS07 [36], who used the same approach, and hence our results share a number of similarities with DSS07 findings. This method was chosen because it is one of the most practical and economic ways to include such uncertainty and in agreement with previous results reported in the literature. However, this method may suffer from a number of pitfalls. One needs to use a rigorous approach and include the full NNFF1.0 uncertainties in the kaon and proton FFs in Eq. (3). In order to ensure the effect of this alternative method on our conclusions, we also examined this approach. Our study shows that one can reach the same conclusions, finding no increase in the size of uncertainty. For the physical parameters, we exactly follow the analysis by the NNFF Collaboration (NNFF1.0). We use the heavy flavor masses for charm and bottom as $m_c = 1.51$ GeV and $m_b = 4.92$ GeV [8,9], respectively. Also, the Z-boson mass is chosen to be $M_Z = 91.187$ GeV, and the QCD coupling constant is fixed to the world average, $\alpha_s(M_Z) = 0.1185$ [56].

Now, we are in a position to present our QCD fit methodology and input functional form, as well as the assumptions we used in our analysis to determine the pion FFs. We choose a flexible input parametrization for pion FFs at an initial scale Q_0, which we also used in our very recent analysis of unidentified light charged hadrons [11]:

$$D_i^{\pi^\pm}(z, Q_0) = \frac{\mathcal{N}_i z^{\alpha_i}(1-z)^{\beta_i}[1 + \gamma_i(1-z)^{\delta_i}]}{B[2 + \alpha_i, \beta_i + 1] + \gamma_i B[2 + \alpha_i, \beta_i + \delta_i + 1]}, \qquad (4)$$

where $i = u^+, d^+, s^+, c^+, b^+$ and g, $q^+ = q + \bar{q}$. In order to normalize the parameter $\mathcal{N}_i$, we use the Euler beta function $B[a, b]$. Since we include the FF sets of NNFF1.0 for the kaon and proton, we choose the initial scale of energy $Q_0 = 5$ GeV, and therefore the number of active flavors in our analyses needs to be fixed at $n_f = 5$. In addition, the charge conjugation and isospin symmetry $D_{u^+}^{\pi^\pm} = D_{d^+}^{\pi^\pm}$ are assumed. More specifically, the γ and δ

TABLE III.   The best-fit parameters for the fragmentation of partons into the $\pi^{\pm}$ for both pion fit and pion + hadron fit analyses at NLO and NNLO accuracy. The starting scale is taken to be $Q_0 = 5$ GeV for all parton species.

Parameter	"Pion" NLO	"Pion" NNLO	"Pion + hadron" NLO	"Pion + hadron" NNLO
$\mathcal{N}_{u^+}$	1.123	1.062	1.133	1.071
α_{u^+}	−0.617	−0.713	−0.558	−0.671
β_{u^+}	1.737	1.854	1.757	1.862
γ_{u^+}	8.324	6.550	9.705	7.742
δ_{u^+}	5.175	5.843	5.314	6.163
$\mathcal{N}_{s^+}$	0.239	0.456	0.124	0.397
α_{s^+}	1.634	0.598	3.376	0.986
β_{s^+}	10.714	8.468	12.658	8.873
$\mathcal{N}_{c^+}$	0.739	0.777	0.724	0.773
α_{c^+}	−0.903	−0.901	−0.929	−0.907
β_{c^+}	4.662	5.055	4.520	4.917
$\mathcal{N}_{b^+}$	0.694	0.735	0.673	0.735
α_{b^+}	−0.395	−0.446	−0.346	−0.449
β_{b^+}	5.346	5.057	4.728	4.500
γ_{b^+}	6.014	7.356	9.098	8.735
δ_{b^+}	9.102	8.567	10.573	9.086
$\mathcal{N}_g$	0.616	0.571	0.705	0.611
α_g	0.406	0.137	−0.230	−0.068
β_g	14.210	16.174	8.658	13.688

parameters for s^+, c^+ and g could not be well constrained by the SIA data, and we are forced to fix them as $\gamma_{s^+,c^+,g} = 0$ and $\delta_{s^+,c^+,g} = 0$. Then the best fit is only achieved with all five parameters of Eq. (4) for u^+ and b^+. We determine 19 free parameters by a standard χ^2 minimization strategy for which the details can be found in Refs. [11,57].

The free parameters are determined from the best fit, and we list them in Table III. In the second and third columns of this table, we report our best-fit parameters for only pion data analysis at NLO and NNLO accuracy, respectively. The parameters reported by the fourth and fifth columns are for analyses with both pion and unidentified hadron datasets at both perturbative orders.

IV. ANALYSIS RESULTS

After the detailed presentation of the experimental datasets included in the present work and the theoretical and phenomenological framework of the analysis in the previous sections, in the following section we present the numerical results obtained for the pion FFs from different analyses and compare them with each other. As we mentioned before, the main goal of the present work is to investigate, for the first time, the impact of unidentified light charged hadron experimental data on the pion FFs at both NLO and NNLO accuracy. In this respect, the pion FFs should be determined by performing two different analyses: (1) The determination of pion FFs through a QCD analysis of only pion datasets as usual (pion fit). (2) The

determination of pion FFs through a simultaneous analysis of both pion and unidentified light charged hadron datasets (pion + hadron fit).

The important point that should be noted is the presence of the kaon, proton, and *residual* FFs in the theoretical calculation of the unidentified light charged hadron cross sections, which is required for the second analysis. As discussed in Sec. III, we use the kaon and proton FFs from the NNFF1.0 analysis [9] and ignore the small *residual* contribution. Hence, some theoretical uncertainties should be taken into account in the analysis containing the unidentified light charged hadron data. One of the most common methods is adding a point-to-point uncertainty to the experimental data as a systematic error source, 8% in our analyses.

A. Comparison of χ^2 values

The list of experimental datasets, including their references as well as the results of our analyses introduced above, has been summarized in Tables I and II at NLO and NNLO, respectively. In each table, the second column indicates the kind of observable measured by each experiment, and the third column specifies its related value of the center-of-mass energy. Note also that the columns labeled by "pion" and "pion + hadron" contain the results of the first and second analyses, respectively. The values of χ^2 per number of data points (χ^2/N_{pts}) have been presented in these columns for each dataset. Moreover, the value of total χ^2 divided by the number of degrees of freedom ($\chi^2/\text{d.o.f.}$) for each analysis is presented in the last row of the table. The total number of data points included in the "pion fit" analysis is 405, while it is 879 for the "pion + hadron fit" analysis. According to the results obtained, the following conclusions can be drawn: For the case of NLO analyses, although the values of χ^2/N_{pts} have increased almost for each pion dataset after the inclusion of the unidentified light charged hadron data, the values of $\chi^2/\text{d.o.f.}$ for the "pion fit" and "pion + hadron fit" analyses are almost equal. Such behavior is seen for some of the datasets in the case of NNLO analyses, but with the difference that the value of $\chi^2/\text{d.o.f.}$ has decreased by including the unidentified light charged hadron data in the analysis. Another point that should be noted here is the significant reduction in the value of $\chi^2/\text{d.o.f.}$ when we move from NLO to NNLO. The optimum values of fit parameters have been presented in Table III, where the first and second columns are related to the pion data analyses at NLO and NNLO, respectively, while the third and fourth columns contain the results of the simultaneous analyses of the pion and hadron data at NLO and NNLO accuracy.

B. Comparison of the relative uncertainties

In order to investigate the impact arising from the inclusion of unidentified light charged hadron experimental

data on pion FFs in both behavior and uncertainty, the results obtained from the "pion fit" and "pion + hadron fit" analyses can be compared in various ways. One of the best approaches to check the validity and excellency of the new results obtained, specifically in view of the uncertainties, is comparing the relative uncertainties of the extracted distributions which are obtained, for each analysis separately, by dividing the upper and lower bands by the central values. Figure 1 shows a comparison between the relative uncertainties of pion FFs obtained from the "pion fit" and "pion + hadron fit" analyses at NLO accuracy. We have presented the results for all flavors parametrized in the analysis at the initial scale of $Q_0 = 5$ GeV. As can be seen,

except for the case of $s + \bar{s}$ FF, the relative uncertainties of pion FFs obtained from the simultaneous analysis of the pion and hadron data are smaller than those obtained by fitting the pion data alone, especially for the case of gluon FFs. In fact, the amount of uncertainty of the $s + \bar{s}$ FF from "pion + hadron fit" analysis is also less than that from "pion fit" analysis (as will be shown later), but since its central value is smaller by a factor of 2, it has overall a relative uncertainty which is somewhat larger.

Figure 2 shows the same results as Fig. 1, but this time for our NNLO analysis. One can clearly conclude that the inclusion of the unidentified light charged hadron data in the pion FF analysis at NNLO accuracy can also lead to a
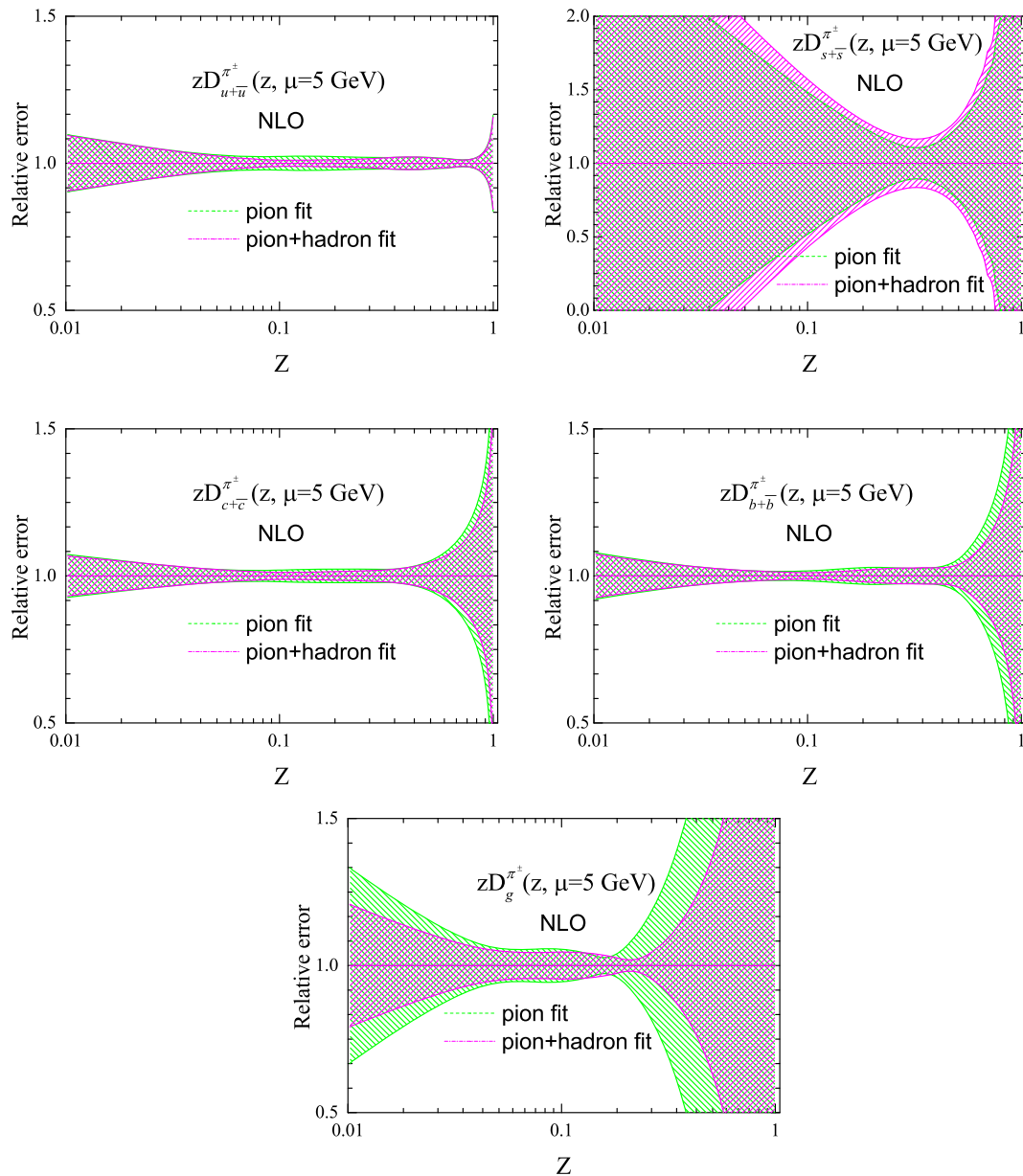
FIG. 1.   Comparison between the relative uncertainties of pion FFs at $Q_0 = 5$ GeV obtained from the "pion fit" and "pion + hadron fit" analyses at NLO.

smaller relative uncertainty for all flavors. Note that, compared with the NLO results, the relative uncertainty of the $s + \bar{s}$ FF from "pion + hadron fit" analysis has now remarkably decreased at lower z values compared to its distribution from "pion fit" analysis. Overall, the results obtained indicate that by performing a simultaneous analysis of pion and unidentified light charged hadron data, a pion FFs set with more acceptable uncertainties can be obtained at both NLO and NNLO accuracies.

To study the effects of the evolution and also evaluate the results at a given higher energy, we recalculate the predictions of Figs. 1 and 2, but this time for $Q = M_z$. The results obtained have been shown in Figs. 3 and 4 at NLO and NNLO, respectively. The reduction in the relative

uncertainty of all flavors after the inclusion of the unidentified light charged hadron data in the analysis is clearly seen from these figures. Note that the shift observed in the relative uncertainty of $s + \bar{s}$ and gluon FFs from "pion + hadron fit" analysis compared with those from "pion fit" analysis at NLO (see Fig. 3) is due to the considerable change in the central values of these distributions after the inclusion of the hadron data.

Another way of comparing the results of two aforementioned analyses is using the ratio plots in which any change in the central values of the distribution can be also investigated, in addition to their uncertainties. Figure 5 shows a comparison between the ratios of pion FFs obtained from the "pion + hadron fit" analysis (yellow
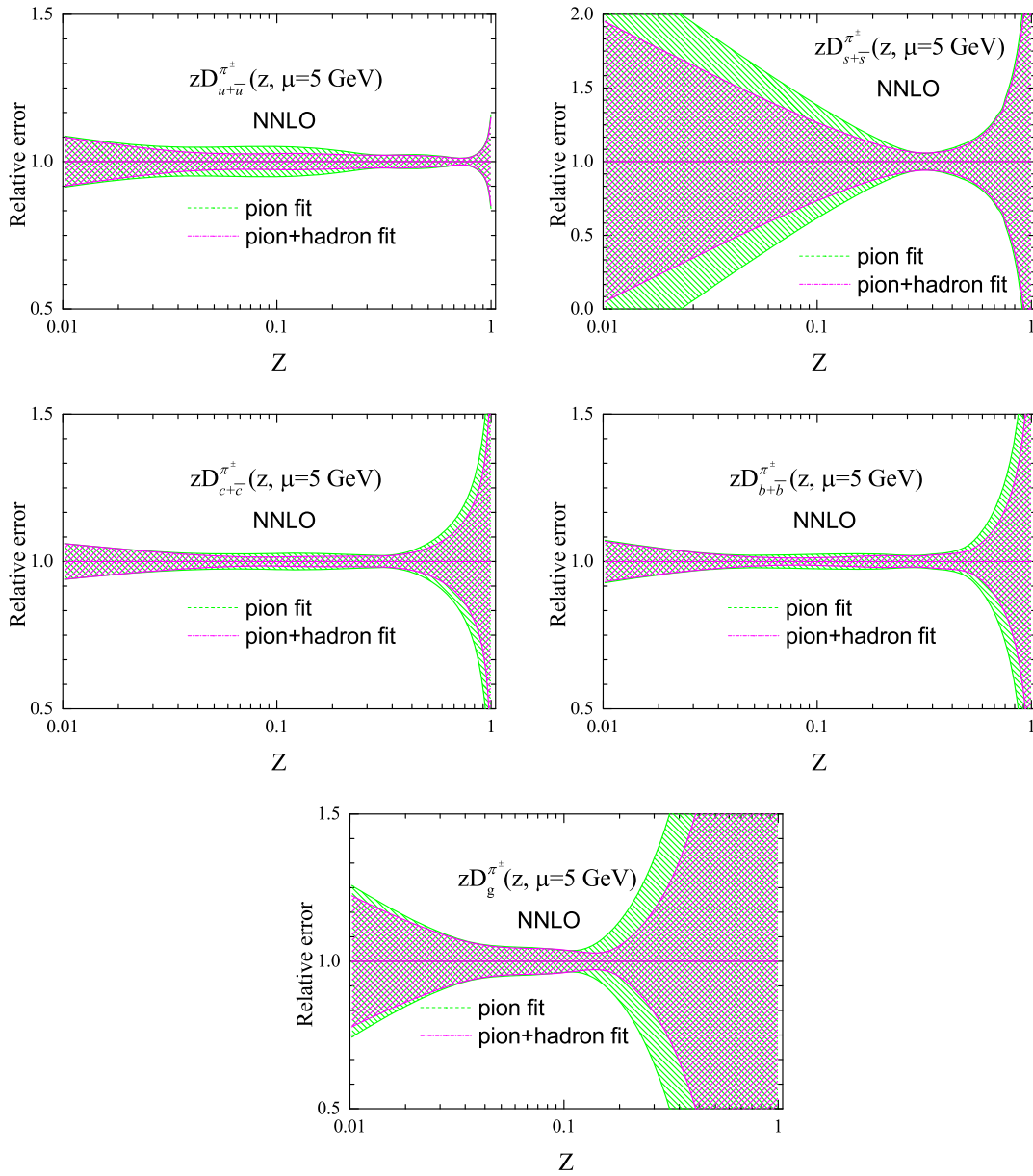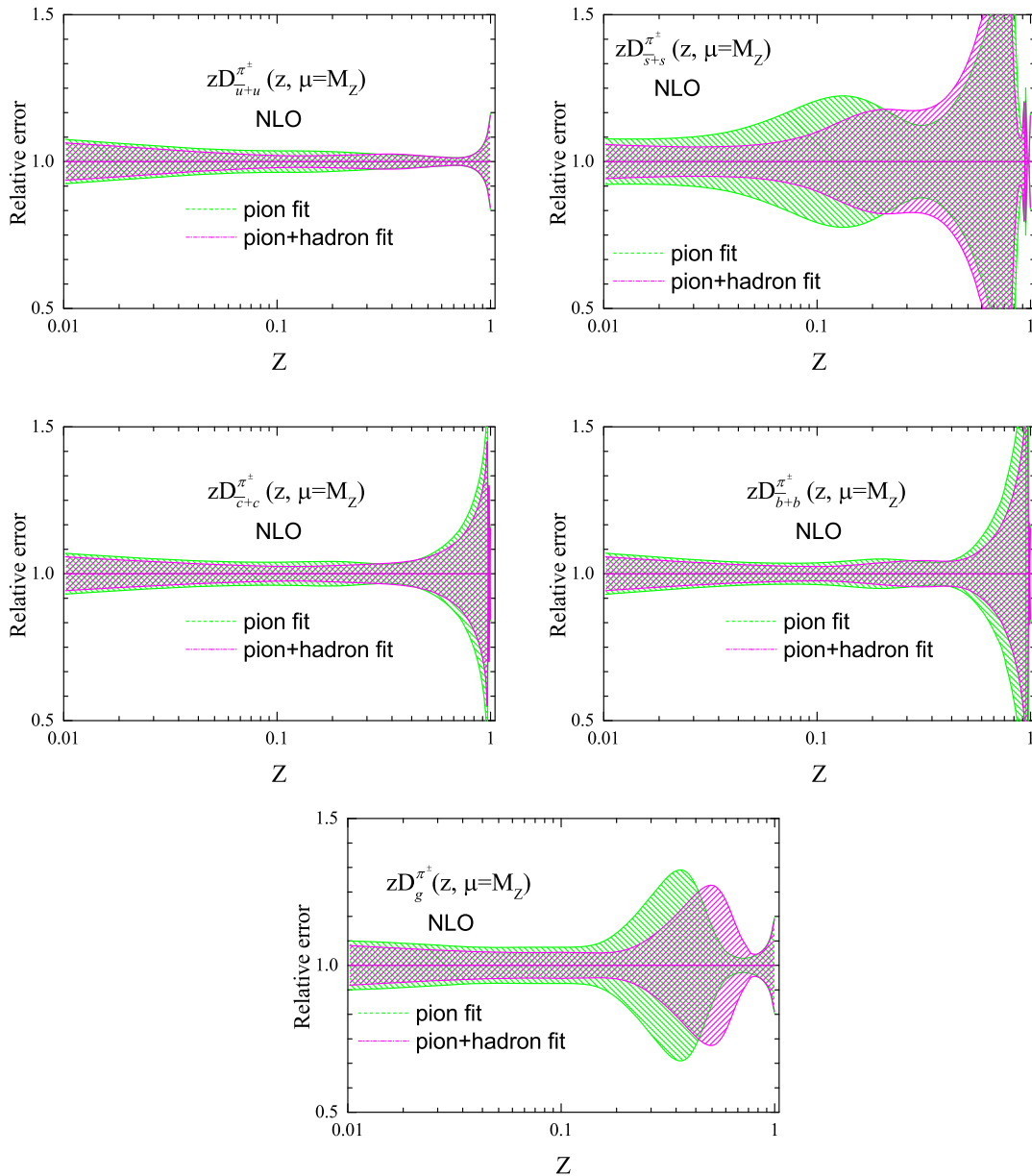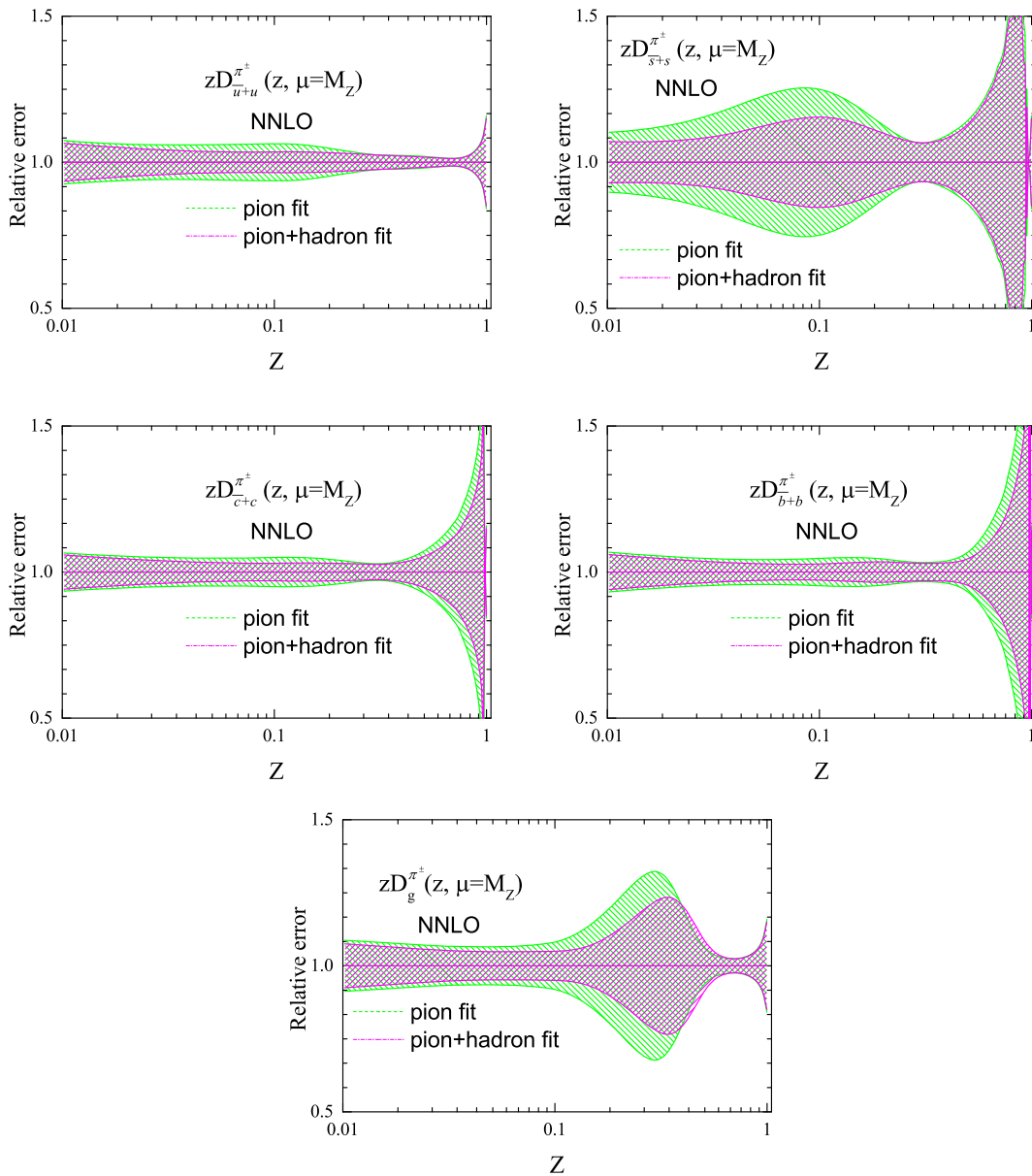

FIG. 2. Same as Fig. 1, but at NNLO.

FIG. 3.   Same as Fig. 1, but at $Q = M_Z$.

band) and also from NNFF1.0 [9] (green band) to those obtained from the "pion fit" analysis (blue band) at $Q = M_z$ and NLO. According to the results obtained, one can see that the uncertainties of all flavor distributions have been decreased by the inclusion of the unidentified light charged hadron data in the analysis compared with the "pion fit" analysis. Overall, our FFs, whether from the "pion fit" analysis or the "pion + hadron fit" one, have smaller uncertainties than the NNFF1.0 results, especially for the cases of up, strange, and gluon distributions.

Let us focus on each flavor separately to discuss the changes in more details. For the case of $u + \bar{u}$ FF, no significant change can be seen between the "pion fit" and "pion + hadron fit" analyses. However, both of these analyses have different results from the $u + \bar{u}$ FF of NNFF1.0, almost for all values of z. Actually, the difference is more significant at lower values of z and reaches even to 30%. The second panel of Fig. 5 shows that the inclusion of hadron data in the analysis of pion FFs at NLO can put further constraints on $s + \bar{s}$ FFs, especially at medium- to small-z regions, so that the uncertainty is remarkably reduced. Moreover, it decreases the $s + \bar{s}$ distribution in magnitude at medium and large values of z. It should be noted that our results for the $s + \bar{s}$ FF are very different from the NNFF1.0 result and have smaller magnitudes up to 100% at smaller z values. For the cases of $c + \bar{c}$ and $b + \bar{b}$ FFs, all three analyses have almost the same results both in magnitude and uncertainties at medium

FIG. 4. Same as Fig. 1, but for $Q = M_Z$ at NNLO.

to small values of z, but they differ at larger values. To be more precise, the $c + \bar{c}$ FFs of the "pion fit" and "pion + hadron fit" analyses are similar even at large values of z, but the NNFF1.0 result grows rapidly in this region. In contrast, the $b + \bar{b}$ FF of "pion + hadron fit" analysis behaves more similarly to the NNFF1.0 and grows rapidly at large z values compared with the "pion fit" analysis. Overall, one can conclude that the inclusion of the hadron data in the analysis does not affect the $c + \bar{c}$ FF, but it can change the $b + \bar{b}$ FF at large values of z. The last panel of Fig. 5 shows again the immense impact of the unidentified light charged hadron data on the gluon FFs of pions, especially at medium values of z. As can be seen, in addition to the significant reduction of the gluon FF uncertainty, its central value has changed considerably at around $z = 0.4$

and has become more consistent with the NNFF1.0 result at this region. However, there are still some differences at $0.1 \lesssim z \lesssim 0.8$, though all three analyses have almost the same results at small z values. Another important point that should be noted is the much lower uncertainty of our results compared with the NNFF1.0 ones—in particular, at large-z regions, which can be attributed to the low flexibility of our parametrization for the gluon FF.

Figure 6 shows the same results as Fig. 5, but at NNLO accuracy. Overall, the interpretation of results obtained for each flavor distribution is similar to the NLO case, with the difference that now the discrepancy observed between the $s + \bar{s}$ and also gluon FFs from the "pion fit" and "pion + hadron fit" analyses at medium-z regions is more moderate than before. For example, the difference between
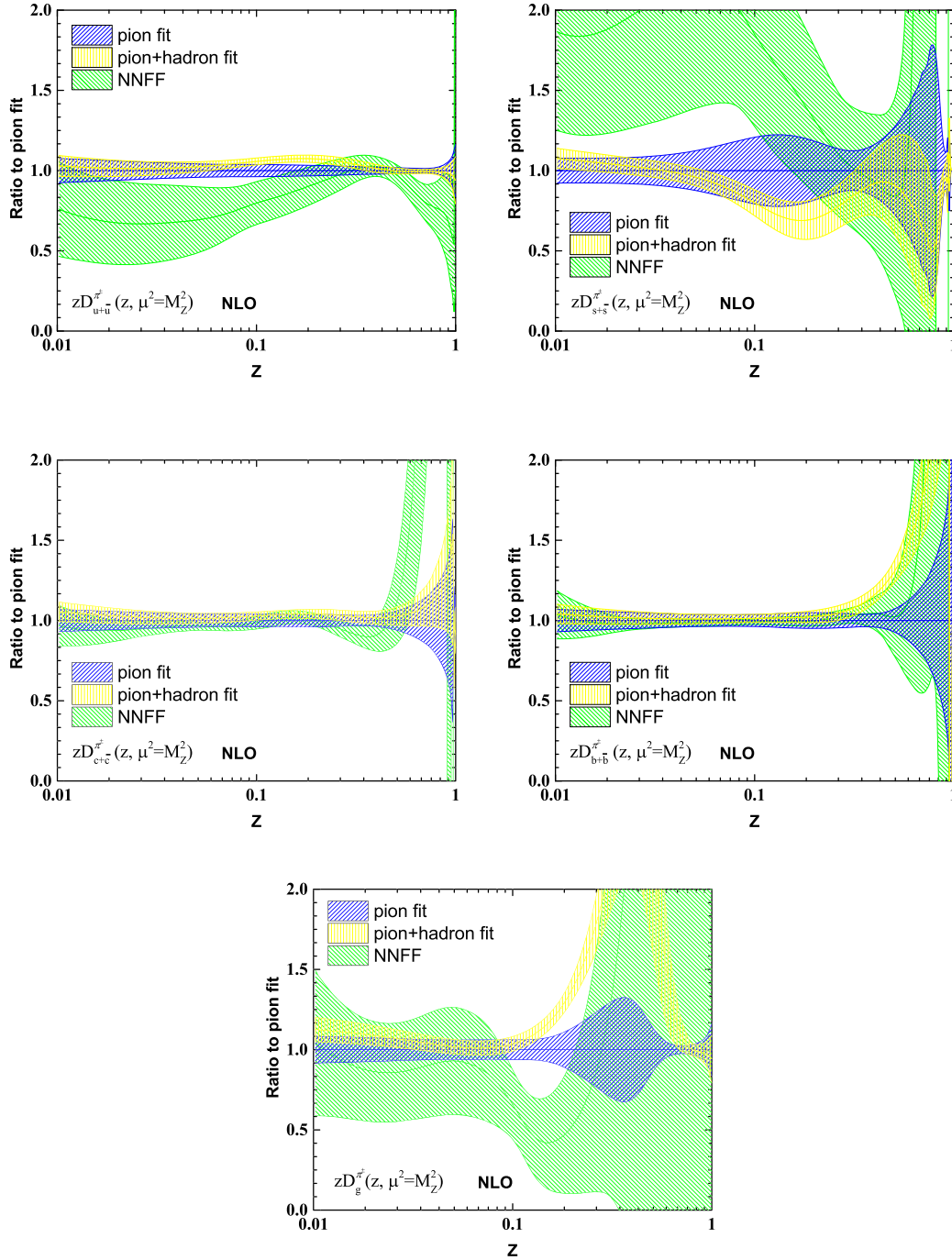
FIG. 5.   Comparison between the pion FFs ratios from the "pion fit," "pion + hadron fit," and NNFF1.0 analyses to the pion FFs from "pion" analysis at NLO for $Q = M_Z$.

the gluon FFs obtained from these two analyses at $z \simeq 0.4$ is less than 50% according to the last panel of Fig. 6, while it is more than 100% at NLO (see Fig. 5). Another point that should be noted is that the $u + \bar{u}$ and $c + \bar{c}$ FFs remain still unchanged after the inclusion of the unidentified light charged hadron data in the analysis, and the $b + \bar{b}$ FF grows rapidly at large z values, similarly to the NLO case.

C. Comparison of the "pion + hadron fit" at NLO and NNLO accuracy

Considering the "pion + hadron fit" analysis as a final and more excellent analysis to determine the pion FFs from SIA data, it is also of interest to compare the distributions obtained at NLO and NNLO accuracy. A comparison between the NLO and NNLO pion FFs determined from a simultaneous analysis of pion and unidentified light
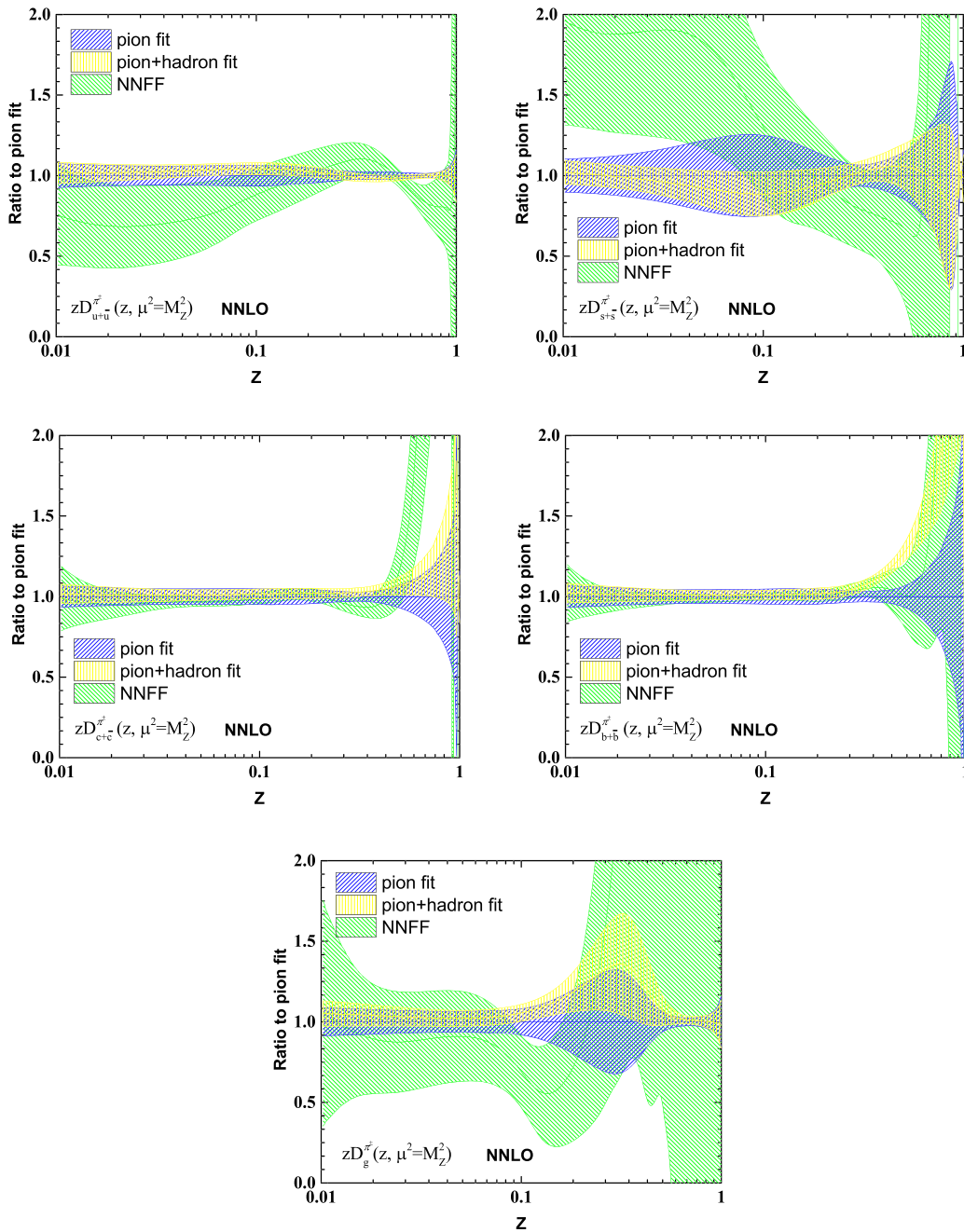
FIG. 6.   Same as Fig. 5, but at NNLO.

charged hadron data for all flavor distributions at $Q_0 = 5$ GeV has been shown in Fig. 7. Overall, we can say that no improvement will be achieved in FF uncertainties by going from NLO to NNLO accuracy. However, there are some crucial changes in the central values of the obtained densities. As can be seen, the $u + \bar{u}$ and gluon FFs follow a similar manner. To be more precise, although the size of the changes is not too large, both of them are increased at smaller values of z and decreased at larger values, since the NNLO corrections are included. The $c + \bar{c}$ and $b + \bar{b}$ FFs are partially changed just at smaller values

of z. But the situation is completely different for the case of the $s + \bar{s}$ FF. Actually, the magnitude of its distribution grows to a great extent by considering the NNLO corrections. Note that, although the uncertainty band of the $s + \bar{s}$ FF at NNLO is bigger than the NLO one, the relative uncertainties of two distributions (similar to Fig. 1) are of the same order.

D. Comparison of the data and theory predictions

Now, we are in a position to complete our study of the fit quality, as well as the data vs theory comparisons.
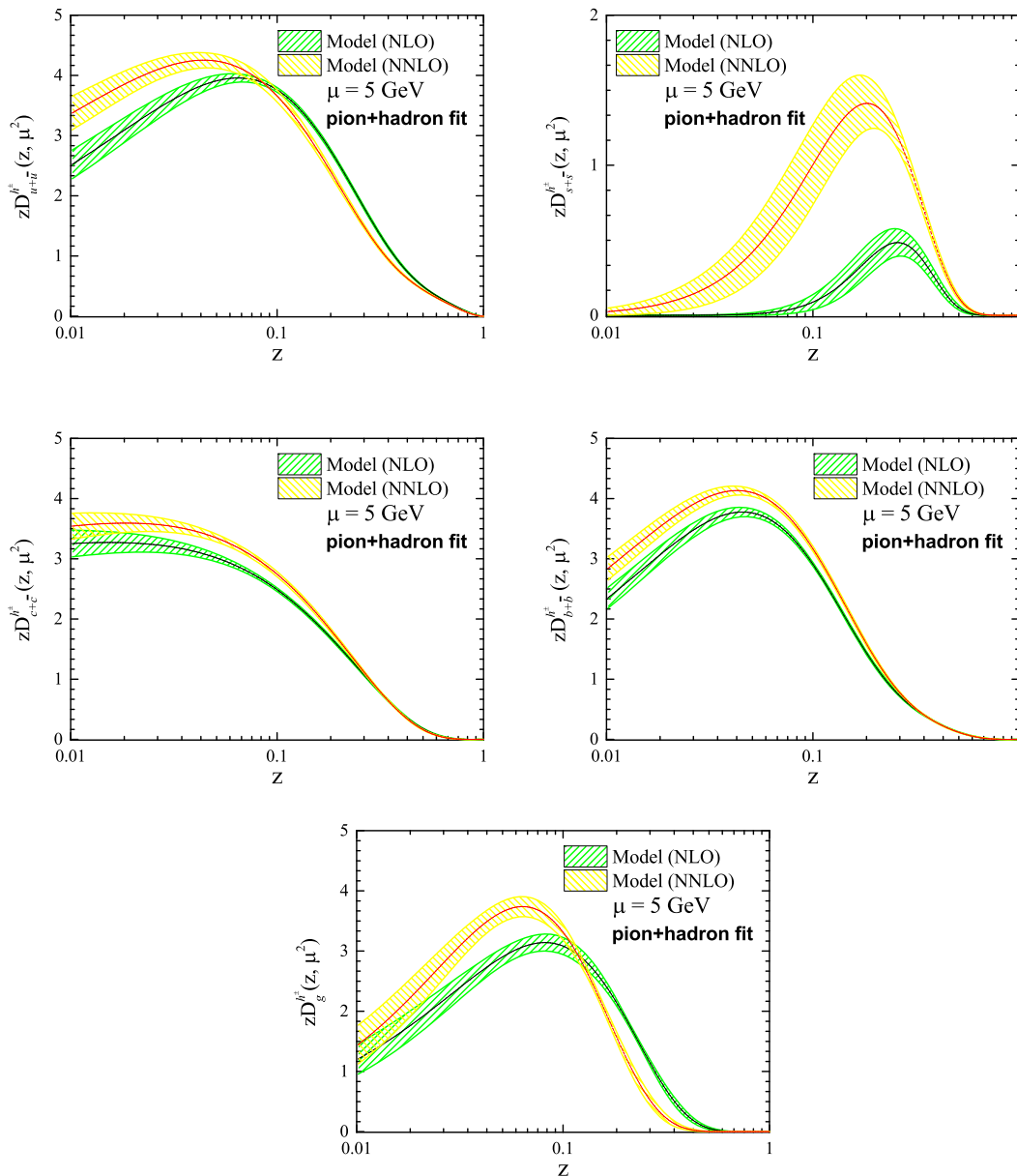
FIG. 7.   Comparison between the NLO and NNLO pion FFs determined from a simultaneous analysis of pion and unidentified light charged hadron data, "pion + hadron fit," for all flavor distributions at $Q_0 = 5$ GeV.

Here we will focus on the theory prediction based on the extracted pion FFs from our "pion + hadron fit" analysis. We turn to consider only the NNLO results to calculate the normalized cross section for the total, light, c-tagged and b-tagged cases. To begin with, in Fig. 8, we show the detailed comparisons of $\frac{1}{\sigma_{\text{tot}}} \frac{d\sigma^{\pi^{\pm}}}{dz}$ with the SIA datasets analyzed in this study. These datasets include the charged pion productions in ALEPH, DELPHI, SLD, and OPAL experiments. As we can see from this comparison, the agreement between the analyzed datasets and theoretical predictions for a wide range of z are excellent, which shows both the validity and the quality of the QCD

fits. In Fig. 9, we show the comparison between the NNLO theory based on our "pion + hadron fit" with the charged pion productions in *BABAR* and Belle experiments. From the comparisons in this figure, we can see again that the data vs theory comparisons are excellent.

As a short summary, considering the impact of these two types of data on the pion FFs, shown in plots presented in this section, one sees that in the case of "pion + hadron fit" analysis, there is a visible reduction on the pion FF uncertainties at a wide range of z, showing that the inclusion of two datasets simultaneously is somewhat more constraining.
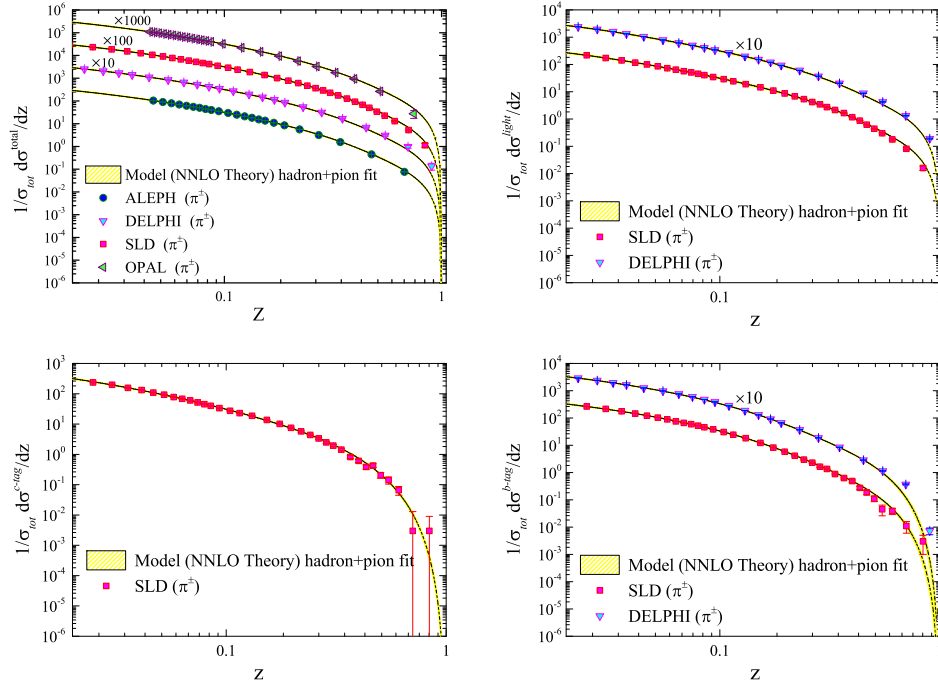
FIG. 8. Detailed comparisons of $\frac{1}{\sigma_{\text{tot}}}\frac{d\sigma^{\pi^{\pm}}}{dz}$ with the SIA datasets for the charged pion productions in ALEPH, DELPHI, SLD, and OPAL experiments.
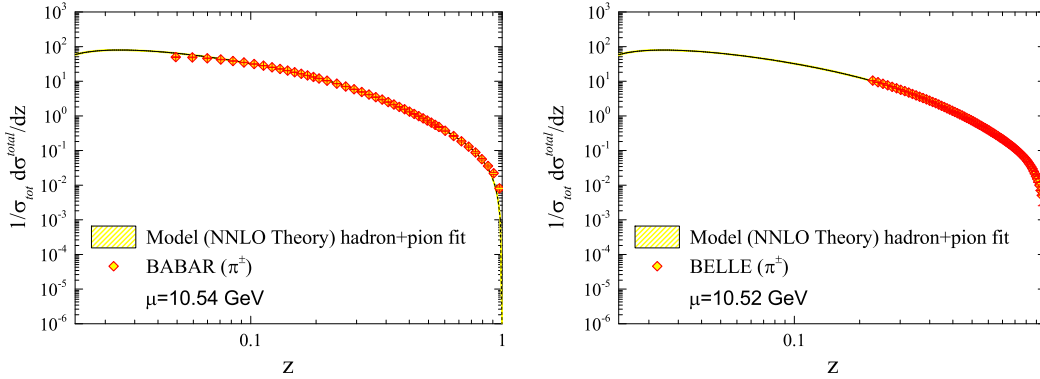

FIG. 9. Detailed comparisons of $\frac{1}{\sigma_{\text{tot}}}\frac{d\sigma^{\pi^{\pm}}}{dz}$ with the SIA datasets for the charged pion productions in *BABAR* and Belle experiments.

V. SUMMARY AND CONCLUSIONS

In this study, we have quantified the constraints that the unidentified light charged hadron datasets could impose on the determination of pion FFs. To achieve this goal, new determinations of pion FFs at NLO and NNLO QCD corrections have been carried out based on comprehensive datasets of SIA processes. In this respect, we calculate the pion FFs from QCD analyses of two different datasets. First, the pion FFs are determined through QCD analyses of pion experimental datasets alone, which are referred to as "pion fit" analyses. In addition to the determination of pion FFs using pion experimental datasets, one may certainly expect further constraints to become available for pion FFs

studies, and improved knowledge of the FFs will become possible from other sources of experimental information. Although the datasets of pion production in electron-positron annihilation include inclusive, uds-tagged, c-tagged, and b-tagged observables, some of the parameters of pion FFs at initial scale cannot be constrained well enough. Since most of the contribution of unidentified light charged hadrons cross sections in SIA measurements is related to the identified pion production, one can expect further constraints by adding these datasets into the QCD fits. Hence, to achieve the first and new determination of pion FFs, we have explicitly chosen our input dataset and calculated pion FFs by adding simultaneously the pion and unidentified light charged hadron datasets in our analysis,

which is called a "pion + hadron fit" analysis. Our main finding is that using the pion experimental data along with the unidentified light charged hadron datasets has the potential to significantly reduce the pion FF uncertainties in a wide kinematic range of momentum fraction z.

According to the plots presented in this study, one can clearly see the reduction of pion FF uncertainties in almost the entire range of z. The largest effects of adding unidentified light charged hadron datasets in a "pion + hadron fit" analysis are seen for the $s + \bar{s}$ and gluon FFs. Not only do the uncertainties of $s + \bar{s}$ and gluons decrease, but also the behavior of their central values changes considerably. Consequently, our study shows that applying unidentified light charged hadron observables together with pion production datasets in a calculation of pion FFs leads to a somewhat better fit quality. Since the higher-order corrections are significant, we plan to study the effect arising from higher-order correction in the determination of pion FFs. Since we include the SIA datasets in our analyses, the perturbative QCD corrections up to NNLO accuracy can be considered. We found that our results at NNLO corrections improved the fit quality in comparison to the NLO accuracy, and that they lead to the reduction of χ^2 for all datasets separately, as well as for the total χ^2. By considering the NNLO corrections, similar slight improvements in the FF uncertainty are also found in some region of z.

The two analyses presented in this study share, however, a common limitation. In both cases, it has indeed been necessary to include other sources of experimental information, such as the data from semi-inclusive deep inelastic scattering (SIDIS), and proton-proton and proton-antiproton collisions measured by TEVATRON, RHIC and LHC. However, the NNLO calculations for such processes are not yet available, which would require a relentless effort for the QCD calculations. It is worth mentioning here that our investigations in this study could be extended to the new determination of kaon and proton FFs by considering the unidentified light charged hadron datasets as well as the identified charged hadron production observables. More detailed discussions of these new determinations of kaon and proton FFs will be presented in our upcoming study.

ACKNOWLEDGMENTS

[1] R. A. Khalek, S. Bailey, J. Gao, L. Harland-Lang, and J. Rojo, Towards ultimate parton distributions at the high-luminosity LHC, Eur. Phys. J. C **78**, 962 (2018).

[2] J. Gao, L. Harland-Lang, and J. Rojo, The structure of the proton in the LHC precision era, Phys. Rep. **742**, 1 (2018).

[3] J. Rojo *et al.*, The PDF4LHC report on PDFs and LHC data: Results from Run I and preparation for Run II, J. Phys. G **42**, 103103 (2015).

[4] S. Forte and G. Watt, Progress in the determination of the partonic structure of the proton, Annu. Rev. Nucl. Part. Sci. **63**, 291 (2013).

[5] R. D. Ball and A. Deshpande, The proton spin, semi-inclusive processes, and measurements at a future electron ion collider, arXiv:1801.04842.

[6] R. D. Ball *et al.* (NNPDF Collaboration), Parton distributions from high-precision collider data, Eur. Phys. J. C **77**, 663 (2017).

[7] S. Alekhin, J. Blmlein, S. Moch, and R. Placakyte, Parton distribution functions, α_s, and heavy-quark masses for LHC Run II, Phys. Rev. D **96**, 014011 (2017).

[8] V. Bertone, N. P. Hartland, E. R. Nocera, J. Rojo, and L. Rottoli (NNPDF Collaboration), Charged hadron fragmentation functions from collider data, Eur. Phys. J. C **78**, 651 (2018).

[9] V. Bertone, S. Carrazza, N. P. Hartland, E. R. Nocera, and J. Rojo (NNPDF Collaboration), A determination of the fragmentation functions of pions, kaons, and protons with faithful uncertainties, Eur. Phys. J. C **77**, 516 (2017).

[10] M. Soleymaninia, H. Khanpour, and S. M. M. Nejad, First determination of D^{*+}-meson fragmentation functions and their uncertainties at next-to-next-to-leading order, Phys. Rev. D **97**, 074014 (2018).

[11] M. Soleymaninia, M. Goharipour, and H. Khanpour, First QCD analysis of charged hadron fragmentation functions and their uncertainties at next-to-next-to-leading order, Phys. Rev. D **98**, 074002 (2018).

[12] A. Mohamaditabar, F. Taghavi-Shahri, H. Khanpour, and M. Soleymaninia, Determination of contributions from residual light charged hadrons to inclusive charged hadrons from e^+e^- annihilation data, arXiv:1808.09255.

[13] M. Hirai, H. Kawamura, S. Kumano, and K. Saito, Impacts of B-factory measurements on determination of fragmentation functions from electron-positron annihilation data, Prog. Theor. Exp. Phys. **2016**, 113B04 (2016).

[14] S. M. M. Nejad, M. Soleymaninia, and A. Maktoubian, Proton fragmentation functions considering finite-mass corrections, Eur. Phys. J. A **52**, 316 (2016).

[15] S. M. M. Nejad and P. Sartipi Yarahmadi, Heavy quark fragmentation functions at next-to-leading perturbative QCD, Eur. Phys. J. A **52**, 315 (2016).

[16] S. M. M. Nejad, NLO QCD corrections to triply heavy baryon fragmentation function considering the effect of nonperturbative dynamics of baryon bound states, Phys. Rev. D **96**, 114021 (2017).

[17] M. Soleymaninia, A. N. Khorramian, S. M. M. Nejad, and F. Arbabifar, Determination of pion and kaon fragmentation functions including spin asymmetries data in a global analysis, Phys. Rev. D **88**, 054019 (2013); Publisher's Note, Phys. Rev. D **89**, 039901(A) (2014).

[18] G. R. Boroun, S. Zarrin, and S. Dadfar, Laplace method for the evolution of the fragmentation function of B_c mesons, Nucl. Phys. **A953**, 21 (2016).

[19] G. R. Boroun, T. Osati, and S. Zarrin, An approximation approach to the evolution of the fragmentation function, Int. J. Theor. Phys. **54**, 3831 (2015).

[20] M. Zarei, F. Taghavi-Shahri, S. A. Tehrani, and M. Sarbishei, Fragmentation functions of the pion, kaon, and proton in the NLO approximation: Laplace transform approach, Phys. Rev. D **92**, 074046 (2015).

[21] D. de Florian *et al.* (LHC Higgs Cross Section Working Group), Handbook of LHC Higgs cross sections: 4. Deciphering the Nature of the Higgs sector, arXiv:1610.07922.

[22] S. Alioli, M. Farina, D. Pappadopulo, and J. T. Ruderman, Precision probes of QCD at high energies, J. High Energy Phys. 07 (2017) 097.

[23] R. D. Ball, S. Carrazza, L. Del Debbio, S. Forte, Z. Kassabov, J. Rojo, E. Slade, and M. Ubiali (NNPDF Collaboration), Precision determination of the strong coupling constant within a global PDF analysis, Eur. Phys. J. C **78**, 408 (2018).

[24] V. N. Gribov and L. N. Lipatov, Deep inelastic $e\,p$ scattering in perturbation theory, Yad. Fiz. **15**, 781 (1972) [Sov. J. Nucl. Phys. **15**, 438 (1972)].

[25] L. N. Lipatov, The parton model and perturbation theory, Yad. Fiz. **20**, 181 (1974) [Sov. J. Nucl. Phys. **20**, 94 (1975)].

[26] G. Altarelli and G. Parisi, Asymptotic freedom in parton language, Nucl. Phys. **B126**, 298 (1977).

[27] Y. L. Dokshitzer, Calculation of the structure functions for deep inelastic scattering and e^+e^- annihilation by perturbation theory in quantum chromodynamics., Zh. Eksp. Teor. Fiz. **73**, 1216 (1977) [Sov. Phys. JETP **46**, 641 (1977)].

[28] N. Sato, J. J. Ethier, W. Melnitchouk, M. Hirai, S. Kumano, and A. Accardi, First Monte Carlo analysis of fragmentation functions from single-inclusive e^+e^- annihilation, Phys. Rev. D **94**, 114004 (2016).

[29] S. Albino, B. A. Kniehl, and G. Kramer, Fragmentation functions for K_S^0 and Λ with complete quark flavor separation, Nucl. Phys. **B734**, 50 (2006).

[30] S. Albino, B. A. Kniehl, and G. Kramer, AKK update: Improvements from new theoretical input and experimental data, Nucl. Phys. **B803**, 42 (2008).

[31] C. A. Aidala, F. Ellinghaus, R. Sassot, J. P. Seele, and M. Stratmann, Global analysis of fragmentation functions for eta mesons, Phys. Rev. D **83**, 034002 (2011).

[32] S. Kretzer, Fragmentation functions from flavor inclusive and flavor tagged e^+e^- annihilations, Phys. Rev. D **62**, 054001 (2000).

[33] B. A. Kniehl, G. Kramer, and B. Potter, Fragmentation functions for pions, kaons, and protons at next-to-leading order, Nucl. Phys. **B582**, 514 (2000).

[34] D. P. Anderle, T. Kaufmann, M. Stratmann, F. Ringer, and I. Vitev, Using hadron-in-jet data in a global analysis of D^* fragmentation functions, Phys. Rev. D **96**, 034028 (2017).

[35] L. Bourhis, M. Fontannaz, J. P. Guillet, and M. Werlen, Next-to-leading order determination of fragmentation functions, Eur. Phys. J. C **19**, 89 (2001).

[36] D. de Florian, R. Sassot, and M. Stratmann, Global analysis of fragmentation functions for protons and charged hadrons, Phys. Rev. D **76**, 074033 (2007).

[37] M. Leitgab *et al.* (Belle Collaboration), Precision Measurement of Charged Pion and Kaon Differential Cross Sections in e^+e^- Annihilation at $\sqrt{s} = 10.52$ GeV, Phys. Rev. Lett. **111**, 062002 (2013).

[38] J. P. Lees *et al.* (*BABAR* Collaboration), Production of charged pions, kaons, and protons in e^+e^- annihilations into hadrons at $\sqrt{s} = 10.54$ GeV, Phys. Rev. D **88**, 032011 (2013).

[39] R. Brandelik *et al.* (TASSO Collaboration), Charged pion, kaon, proton and anti-proton production in high-energy e^+e^- annihilation, Phys. Lett. **94B**, 444 (1980).

[40] M. Althoff *et al.* (TASSO Collaboration), Charged Hadron composition of the final state in e^+e^- annihilation at high-energies, Z. Phys. C **17**, 5 (1983).

[41] H. Aihara *et al.* (TPC/Two-Gamma Collaboration), Charged-Hadron Inclusive Cross Sections and Fractions in e^+e^- Annihiliation at $\sqrt{s} = 29$ GeV, Phys. Rev. Lett. **61**, 1263 (1988).

[42] W. Braunschweig *et al.* (TASSO Collaboration), Pion, kaon and proton cross-sections in e^+e^- annihilation at 34-GeV and 44-GeV center-of-mass energy, Z. Phys. C **42**, 189 (1989).

[43] D. Buskulic *et al.* (ALEPH Collaboration), Inclusive $\pi^\pm$, $K^\pm$, and $(p, \bar{p})$ differential cross-sections at the Z resonance, Z. Phys. C **66**, 355 (1995).

[44] P. Abreu *et al.* (DELPHI Collaboration), $\pi^\pm$, $K^\pm$, p and $\bar{p}$ production in $Z^0 \to q\bar{q}$, $Z^0 \to b\bar{b}$, $Z^0 \to u\bar{u}$, $d\bar{d}$, $s\bar{s}$, Eur. Phys. J. C **5**, 585 (1998).

[45] R. Akers *et al.* (OPAL Collaboration), Measurement of the production rates of charged hadrons in e^+e^- annihilation at the Z^0, Z. Phys. C **63**, 181 (1994).

[46] K. Abe *et al.* (SLD Collaboration), Production of π^+, π^-, K^+, K^-, p and $\bar{p}$ in light (uds), c and b jets from Z^0 decays, Phys. Rev. D **69**, 072003 (2004).

[47] W. Braunschweig *et al.* (TASSO Collaboration), Global jet properties at 14-GeV to 44-GeV center-of-mass energy in e^+e^- annihilation, Z. Phys. C **47**, 187 (1990).

[48] D. Buskulic *et al.* (ALEPH Collaboration), Measurement of α_s from scaling violations in fragmentation functions in e^+e^- annihilation, Phys. Lett. B **357**, 487 (1995); Erratum, Phys. Lett. B **364**, 247(E) (1995).

[49] P. Abreu *et al.* (DELPHI Collaboration), Measurement of the quark and gluon fragmentation functions in Z^0 hadronic decays, Eur. Phys. J. C **6**, 19 (1999).

[50] K. Ackerstaff *et al.* (OPAL Collaboration), Measurements of flavor dependent fragmentation functions in $Z^0 \rightarrow q\bar{q}$ events, Eur. Phys. J. C **7**, 369 (1999).

[51] R. Akers *et al.* (OPAL Collaboration), Measurement of the longitudinal, transverse and asymmetry fragmentation functions at LEP, Z. Phys. C **68**, 203 (1995).

[52] P. J. Rijken and W. L. van Neerven, Higher order QCD corrections to the transverse and longitudinal fragmentation functions in electron-positron annihilation, Nucl. Phys. **B487**, 233 (1997).

[53] A. Mitov and S. O. Moch, QCD corrections to semi-inclusive hadron production in electron-positron annihilation at two loops, Nucl. Phys. **B751**, 18 (2006).

[54] P. J. Rijken and W. L. van Neerven, $\mathcal{O}(\alpha_s^2)$ contributions to the longitudinal fragmentation function in e^+e^- annihilation, Phys. Lett. B **386**, 422 (1996).

[55] V. Bertone, S. Carrazza, and J. Rojo, APFEL: A PDF evolution library with QED corrections, Comput. Phys. Commun. **185**, 1647 (2014).

[56] M. Tanabashi *et al.* (Particle Data Group), Review of particle physics, Phys. Rev. D **98**, 030001 (2018).

[57] H. Khanpour and S. A. Tehrani, Global analysis of nuclear parton distribution functions and their uncertainties at next-to-next-to-leading order, Phys. Rev. D **93**, 014026 (2016).